Carbon Tetragons as Definitive Spin Switches in Narrow Zigzag Graphene Nanoribbons

Ping Cui,[1] Qiang Zhang,[1,2] Hongbin Zhu,[1,2] Xiaoxia Li,[1,2] Weiyi Wang,[1] Qunxiang Li,[1] Changgan Zeng,[1,2,*] and Zhenyu Zhang[1]

[1]*International Center for Quantum Design of Functional Materials (ICQD), Hefei National Laboratory for Physical Sciences at the Microscale, and Synergetic Innovation Center of Quantum Information and Quantum Physics, University of Science and Technology of China, Hefei, Anhui 230026, China*

[2]*Department of Physics, and CAS Key Laboratory of Strongly-Coupled Quantum Matter Physics, University of Science and Technology of China, Hefei, Anhui 230026, China*

(Received 6 August 2015; revised manuscript received 29 October 2015; published 14 January 2016)

Precise spatial control of the spin propagation channels is of fundamental and practical importance in future graphene-based spintronic devices. Here we use first-principles calculations to show that when narrow zigzag graphene nanoribbons are connected to form junctions or superlattices, properly placed square-shaped carbon tetragons not only serve as effective bundles of the two incoming spin edge channels, but also act as definitive topological spin switches for the two outgoing channels. The nanoribbon segments are largely drawn from different acene molecules. We further show that such spin switches can lift the degeneracy between the two spin propagation channels, which enables tunability of different magnetic states upon charge doping. Preliminary experimental supports for the realization of such tetragons connecting nanoribbon segments are also presented.

DOI: 10.1103/PhysRevLett.116.026802

Spin-polarized states harbored by graphene-based material systems are of particular interest due to their potential applications in future spintronic devices [1]. As one example, it was proposed that spin-orbit coupling may lead to the quantum spin Hall effect (QSHE) in graphene, where the spin-up and spin-down carriers move in opposite directions along the same edges [2]. Nevertheless, the extremely weak intrinsic spin-orbit coupling so far has prevented an experimental realization of the QSHE in graphene [3]. Another compelling example is zigzag graphene nanoribbon (ZGNR), where mean-field theoretical studies indicated a singly spin-polarized electronic state propagating along one edge, with an antiparallelly aligned spin state along the opposite edge, resulting in an overall antiferromagnetic (AFM) configuration of the system [4–9]. Such nontrivial spin states are predicted to persist even for the narrowest ZGNRs, i.e., zigzag acene molecules with finite or infinite lengths [10–12]. Moreover, these one-dimensional (1D) carbon systems have higher spin wave stiffness than traditional magnetic materials, and thus possess relatively long spin correlation lengths [13]. Electric or magnetic fields [7,14–16], edge engineering [17,18], and carrier doping [19] can be exploited to further enrich the degrees of magnetic ordering, for example, into ferromagnetic (FM), half metallic, or spin semiconducting states, offering new opportunities for sp-electron-based spintronics [20].

Aside from modifications of the overall magnetic properties of the ZGNRs, precise control of a specific spin channel via local atomic-scale manipulations is also highly desirable. In this regard, it has been shown that one of the spin channels can be suppressed by selective roughening or adatom adsorption at a given edge, while the other spin channel remains largely intact and can act as an effective spin injector [21,22]. Furthermore, in development of future graphene-based full-scale functional spintronic devices, a prerequisite is to demonstrate the realization of various elemental building blocks for spin logic operations. Pioneering efforts included theoretical demonstrations of several elemental spin logic devices based on the magnetic properties of properly tailored graphene nanostructures [23,24]. Related demonstrations include the operating principles of topological current splitters using graphene junctions [25,26].

In this Letter, we present the first-known design of a topological spin switch in ZGNRs, an indispensable building block in future graphene-based spintronic devices. We reveal that the carbon tetragons properly incorporated in the ZGNRs effectively switch the spin orientation at each edge. We further show that such spin switches can lift the degeneracy between the two spin propagation channels, which enables tunability of different magnetic states upon charge doping. Preliminary experimental supports for the realization of such tetragons connecting nanoribbon segments are also presented, as synthesized by cyclodehydrogenation of pentacenes on a Au(110) surface.

Before going into any details, here we note that the present study is carried out primarily using first-principles calculations within density functional theory (DFT). Previous work based on higher-level methods predicted a singlet ground state with radical character for long-chain acenes [27,28]. These results seem to suggest that the

ground state should be the quantum superposition of the two degenerate AFM states, which otherwise cannot be captured by the standard mean-field DFT calculations with quantum fluctuation disregarded. Moreover, a recent theoretical study of graphene nanoribbons based on an effective quantum Heisenberg model suggested an entangled spin singlet ground state [29], consistent with the rigorous Lieb's thereom [30]. This study further demonstrated that such coherent superposition or entanglement is usually sustained in undisturbed ideal systems [29]. For a realistic system, decoherence effects due to coupling with the environment may dominate, and the quantum superposition or entanglement state eventually collapses into one of the decoherent states [29], such as the static spin polarization state emphasized in the present DFT study.

A graphene sheet consists of two sublattices, and the carbon atoms at the opposite edges of a ZGNR belong to different sublattices as shown in Fig. 1(a). In such a conjugated π-bonded hydrocarbon system, the AFM coupling between the opposite edge states originates from the spin alternation rule for the stabilization of unpaired electrons, resulting in FM (AFM) spin couplings between atoms belonging to the same (different) sublattices [31,32]. Here we consider a square-shaped carbon tetragon connecting the acene molecules (or, equivalently, the narrowest ZGNRs), with the tetragon asymmetrically placed at the corner as depicted in Fig. 1(b). Such a carbon tetragon is expected to mutually switch the sublattice affiliations of the connected two ZGNRs. According to the spin alternation rule [31,32], the spin orientations of the two edge channels should also be switched. In order to validate the above conjectures quantitatively, we use first-principles calculations within spin-polarized DFT to explore a series of acene dimers, acene polymers, and acene superlattices, connected by the carbon tetragons, with the calculation details described in the Supplemental Material [33].

We first investigate different acene dimer configurations, with each dimer consisting of a carbon tetragon connecting two acenes. For short acenes such as anthracene and tetracene, the ground states of their dimers are nonmagnetic (NM). For longer acene building blocks containing at least five fused hydrogen-passivated hexagons (such as pentacene and hexacene), the ground states of the acene dimers are AFM. For example, for a pentacene dimer [Fig. 2(a)], the AFM state is 31 meV lower than the NM state. Figure 2(b) shows the spatial distributions of the spin-dependent highest occupied molecular orbitals (HOMOs) and lowest unoccupied molecular orbitals (LUMOs). The spin-up HOMO is located at the bottom edge of the left acene and switches to the top edge of the right acene, while the spin-down HOMO is located at the top edge of the left acene and switches to the bottom edge of the right acene. Our detailed calculations further show that the spin switching behavior is also observed for the LUMOs. Therefore, the carbon tetragons serve as effective bundles of the two incoming spin edge channels, and further act as definitive topological spin switches to effectively control the trajectories of the spin edge channels. From the naked eye, the HOMO and LUMO look symmetric with respect to the spin inversion, which can be largely attributed to the comparably dominant contributions from the carbon π orbitals. However, these levels actually differ at a precise quantitative level, as reflected in the charge density distributions [Fig. 2(b)] and energy-dependent transmission coefficients (Fig. S1 [33]).

Before considering other configurations, here we emphasize on another subtle but important aspect of the acene dimers connected by the spin switches. As illustrated by the first example of the pentacene dimer [Fig. 2(b)], the spatial symmetry is broken for either the HOMOs or LUMOs with opposite spin orientations, therefore lifting their spin degeneracy. This is confirmed quantitatively by the calculated spin-polarized electronic structure shown in Fig. 2(c), and the energy splitting between the spin-up and spin-down HOMOs is 38 meV. This intriguing aspect will be exploited later to realize other magnetic states, including, in particular, half metallic states.

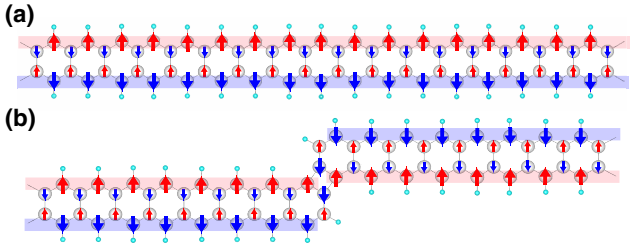

FIG. 1. Schematic spin configurations of different ZGNRs (a) without and (b) with a carbon tetragon as a spin switch.

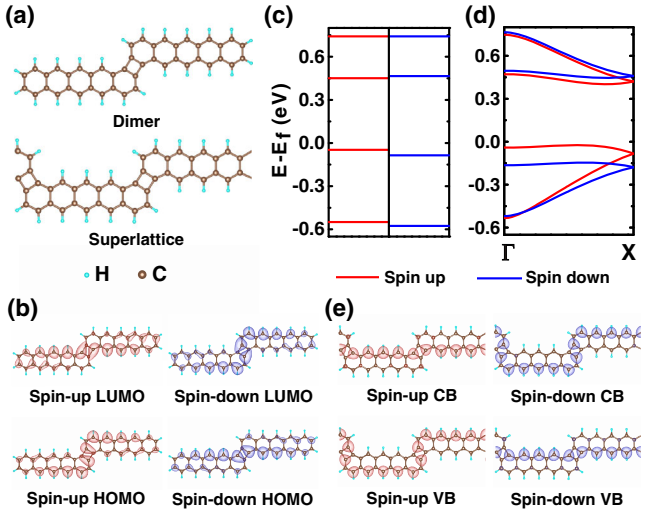

FIG. 2. (a) Optimized atomic structures of a pentacene dimer and a horizontally aligned pentacene superlattice, respectively. (b),(c) The partial charge density distributions and electronic structure of a pentacene dimer. (d),(e) The electronic structure and partial charge density distributions of a pentacene superlattice.

Similar to the symmetric acene dimers, the ground states of asymmetric acene dimers consisting of one-tetragon-connected inequivalent acene building blocks and acene polymers containing multiple carbon tetragons are also found to be AFM. Several specific configurations are given in Fig. S2 [33]. For all these structures, the spin orientations along the two edges always switch across the carbon tetragons.

So far, we have limited our attention to the roles of carbon tetragons as spin switches in different acene dimers and polymers. Next, we generalize to explore the potential effects of the spin switches in graphene superlattices, which may develop emergent quantum phenomena beyond pristine graphene [41,42]. Using the example of pentacenes as building blocks, there are two types of alignments when the pentacenes are connected by the tetragons: horizontal [where the pentacene axis is along the superlattice direction as shown in Fig. 2(a)], or vicinal (where the pentacene axis is tilted away from the superlattice direction). For the first case, it has an AFM ground state, 152 meV per unit cell lower than the FM state and 158 meV lower than the NM state. The energy gains are much larger in the present superlattice case than the earlier acene dimer cases. The spatial distributions of the spin-polarized valence bands (VBs) and conductance bands (CBs) are shown in Fig. 2(e), and the spin orientation is also switched across a carbon tetragon for each band. Strikingly, such spin switching effects lead to substantially different spatial trajectories for each spin channel: Now the spin-down VB (spin-up CB) is spatially confined along a geometrically straight line, while the spin-up VB (spin-down CB) is spatially confined along an armchair curve. In strong contrast, we note that each spin channel is always confined at one edge for pristine ZGNRs, lacking switching capabilities.

In analogy to the acene dimers, the degeneracy is also lifted for the spin-polarized bands [Fig. 2(d)], especially for the VBs, with a spin splitting energy of 95 meV, tripled from the dimer case. These important findings are generic, as demonstrated by the horizontally aligned superlattices consisting of anthracenes, tetracenes, and hexacenes as building blocks (see Fig. S3 in the Supplemental Material [33]). It is worthwhile to point out the added advantage of the superlattice cases, reflected by the fact that the AFM ground states can now also be stabilized for the superlattices consisting of shorter acenes such as anthracenes and tetracenes, even though their dimer configurations favor NM ground states. For the vicinally aligned superlattices such as those consisting of pentacenes shown in Fig. S4 [33], the spin-resolved properties are very similar to that of the horizontally aligned counterparts, with one crucial (and for practical reasons highly undesirable) exception: The spin degeneracy stays intact because the spin configurations of the spin-up and spin-down channels are identical as ensured by the spatial translational symmetry.

To demonstrate the broad applicability of the switching role of the carbon tetragons, we now investigate horizontally aligned superlattices containing two different building blocks whose total length is 10 fused hydrogen-passivated hexagons, but with a carbon tetragon inserted at different locations. The three new and distinct configurations are displayed in Fig. S5 [33], and our calculations show that all these superlattice structures have AFM ground states, with the spin channels along the two edges switched across the carbon tetragons. The spin degeneracies are also lifted in the spin-polarized electronic structures. Furthermore, the spin switching roles of the carbon tetragons are not only valid for the narrowest ZGNRs or their segments, but also effective for ZGNRs or their segments with wider widths, as demonstrated using the example shown in Fig. S6 [33].

To further contrast the distinctive role of the properly positioned carbon tetragons as spin switches, we have also considered several other configurations, in which either a misplaced carbon tetragon or other carbon connectors such as carbon hexagons fail to serve as spin switches. Some representative examples are given in Fig. S7 of the Supplemental Material [33]. For example, when a pentacene dimer or superlattice is symmetrically connected by a carbon tetragon or tetragons, the NM ground state is favored, leaving no opportunity for spin switching and manipulations.

The spin switching and degeneracy lifting roles of the carbon tetragons in different ZGNR structures can be exploited for spintronic device applications. Here we use a horizontally aligned pentacene superlattice to demonstrate the tunable properties of such systems upon hole doping. Without doping, the superlattice is an insulator [see Fig. 2(d)]. When holes are doped into the system, the Fermi level moves down, and the spin splitting at the Γ point first increases from 95 meV at zero doping [Fig. 2(d)] to 170 meV at the hole doping of −1.0 electron/unit cell, and then decreases to 116 meV at −1.7 electrons/unit cell, as shown in Fig. 3(a). In particular, when the hole doping level is in the range around −1.0 electron/unit cell, the

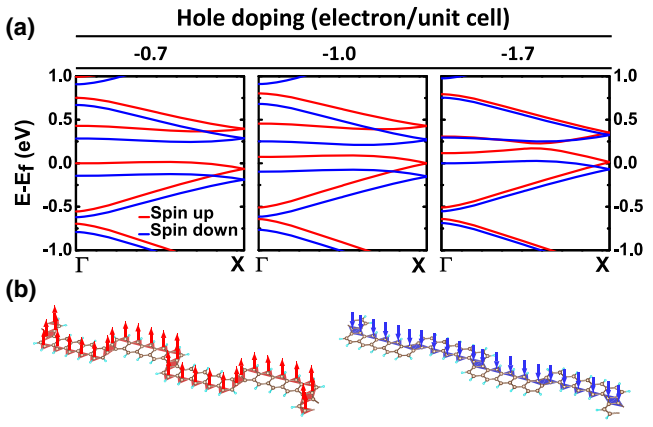

FIG. 3. (a) Spin-polarized band structures of a horizontally aligned pentacene superlattice with hole dopings of −0.7, −1.0, and −1.7 electrons per unit cell. (b) Schematic spatial distributions of the spin-polarized edge states in the superlattice.

Fermi level only crosses the spin-up VB, thereby stabilizing a half metallic state which is further confirmed by the spin transport calculations as shown in Fig. S1 [33]. When the doping level is further increased to be above -1.7 electrons per unit cell, the Fermi level crosses both the spin-up and spin-down VBs, rendering the system to be a unique FM metal. For the half metallic case, the conducting spin-up channel possesses an overall armchair-shaped contour. The unique aspect of the FM metal is characterized by having both conducting spin channels, with the spin-up channel along an armchair-shaped contour, while the spin-down channel along a straight line [Fig. 3(b)]. The spin-dependent spatial distributions of the two spin channels controlled by the inserted carbon tetragons differ substantially from the half metallic and spin-gapless semiconducting states studied previously in graphene nanoribbons [7,17,18], where each spin channel is always localized along one given edge. The topologically controllable spin propagation channels at the ZGNR edges using the carbon tetragons may enable a spectrum of applications in spintronics and quantum computing at the atomic scale.

The strong predictions made so far in the present study are expected to stimulate experimental efforts aimed to establish the various spintronic properties of such ZGNR structures. As preliminary efforts, here we present experimental results to demonstrate that 1D pentacene junctions with carbon tetragons as connectors can be prepared using a self-assembly synthesis technique on a reconstructed Au template [43]. First, submonolayer pentacene molecules were deposited onto a clean Au(110) surface at room temperature. The STM image [Fig. S8(a) [33]] reveals that the molecules form head-to-head chains in the induced (1×3) troughs along the $[11\bar{0}]$ direction, similar to previous observations [44]. Upon subsequent annealing at 350 °C for 2 h, some of the molecules are polymerized into longer chains [Fig. S8(b) [33]]. The high-resolution STM images [Figs. 4(a) and 4(c)] further reveal that the pentacene polymers of different lengths are in armchair shapes. It is thus likely that the pentacenes are connected via the formation of carbon tetragons located at the corners of neighboring pentacenes. Previous theoretical and experimental studies have shown that the acene molecules can be connected by carbon tetragons via cyclodehydrogenation, but the main reaction sites are the central benzene rings of the pentacene molecules [45,46]. Here the petancene molecules are lying head-to-head in the troughs at the Au(110) surface, so that head-on cyclodehydrogenation reactions can now only take place.

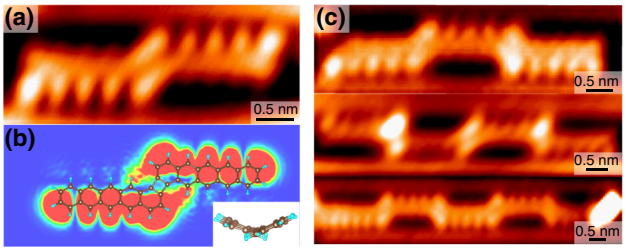

FIG. 4. (a) STM image of a pentacene dimer on the Au(110)–(1×3) surface at sample bias V_s of −1.0 V. (b) Simulated STM image of a V-shaped pentacene dimer at V_s of −1.0 V. The inset is the side view of this dimer structure. (c) STM images of a horizontally aligned pentacene trimer, tetramer, and pentamer on the Au(110)–(1×3) surface at V_s of −1.0, −2.0, and −1.0 V, respectively.

To further support the above picture, we have simulated the constant-height STM image of two pentacene molecules connected at the corner by a carbon tetragon, whose structure is initially optimized on a Au(110)–(1×3) reconstructed surface (Fig. S9 [33]). The simulated STM image is shown in Fig. 4(b), which reproduces well the experimental data. It is noted that the (1×3) troughs at the Au(110) surface are V shaped [47], so that the armchair-shaped pentacene polymers cannot lie flat in the troughs. Instead, the neighboring pentacene segments lie on the opposite walls of the troughs, as evidenced from the optimized V-shaped structure on the theory side and the weak intensity along the inner edges of the pentacene segments on the experimental side (Fig. 4). We have also measured experimentally the intermolecular distance perpendicular to the trough direction, given by 0.26 ± 0.02 nm, which is consistent with the calculated value of 0.26 nm for the optimized structure, confirming that the pentacene polymers are indeed not lying flat on the surface. These findings also rule out the possibility that the pentacene molecules are connected via a single C-C bond formation, which would otherwise result in an intermolecular distance of only 0.20 nm even in the flat-lying configuration. The measured spectroscopy shows an energy gap, similar to those in previous reports of pristine graphene nanoribbons [48]. Finally, we note that direct validations of the AFM ground state and precise spin switching aspects are beyond the experimental capabilities of the present study.

In summary, we have demonstrated that when properly introduced to connect ZGNRs or their segments, carbon tetragons can serve as definitive spin switches to reverse the spin orientations of the two edge channels. This switching effect is observed with a large variety of nanoribbon segments. We have further shown that such spin switches effectively lift the spin degeneracy, which enables tunability of the systems into different magnetic states upon hole doping, including intriguing half metallic and FM configurations. The experimental realization of such graphene nanoribbons connected by carbon tetragons has also been demonstrated by 1D confined reactions via self-assembly. Collectively, the present study offers new insights and opportunities for developing graphene-based spintronics.

This work was supported in part by the National Key Basic Research Program (No. 2014CB921100), by the

Strategic Priority Research Program (B) of the CAS (No. XDB01020000), by the National Natural Science Foundation of China (No. 11434009, No. 11374279, No. 61434002, No. 11204286, No. 21273208, and No. 11461161009), and by the Fundamental Research Funds for the Central Universities (No. WK2030020027).

*Corresponding author.
cgzeng@ustc.edu.cn

[1] O. V. Yazyev, Rep. Prog. Phys. **73**, 056501 (2010).
[2] C. L. Kane and E. J. Mele, Phys. Rev. Lett. **95**, 226801 (2005).
[3] H. Min, J. E. Hill, N. A. Sinitsyn, B. R. Sahu, L. Kleinman, and A. H. MacDonald, Phys. Rev. B **74**, 165310 (2006).
[4] M. Fujita, K. Wakabayashi, K. Nakada, and K. Kusakabe, J. Phys. Soc. Jpn. **65**, 1920 (1996).
[5] S. Okada and A. Oshiyama, Phys. Rev. Lett. **87**, 146803 (2001).
[6] H. Lee, Y.-W. Son, N. Park, S. Han, and J. Yu, Phys. Rev. B **72**, 174431 (2005).
[7] Y.-W. Son, M. L. Cohen, and S. G. Louie, Nature (London) **444**, 347 (2006).
[8] L. Pisani, J. A. Chan, B. Montanari, and N. M. Harrison, Phys. Rev. B **75**, 064418 (2007).
[9] J. Jung, T. Pereg-Barnea, and A. H. MacDonald, Phys. Rev. Lett. **102**, 227205 (2009).
[10] M. Bendikov, H. M. Duong, K. Starkey, K. N. Houk, E. A. Carter, and F. Wudl, J. Am. Chem. Soc. **126**, 7416 (2004).
[11] D.-E. Jiang and S. Dai, J. Phys. Chem. A **112**, 332 (2008).
[12] R. Pilevarshahri, I. Rungger, T. Archer, S. Sanvito, and N. Shahtahmassebi, Phys. Rev. B **84**, 174437 (2011).
[13] O. V. Yazyev and M. I. Katsnelson, Phys. Rev. Lett. **100**, 047209 (2008).
[14] E. J. G. Santos, J. Phys. Chem. C **117**, 6420 (2013).
[15] W. Y. Kim and K. S. Kim, Nat. Nanotechnol. **3**, 408 (2008).
[16] F. Muñoz-Rojas, J. Fernández-Rossier, and J. J. Palacios, Phys. Rev. Lett. **102**, 136810 (2009).
[17] E.-J. Kan, Z. Y. Li, J. L. Yang, and J. G. Hou, J. Am. Chem. Soc. **130**, 4224 (2008).
[18] Z. F. Wang, S. Jin, and F. Liu, Phys. Rev. Lett. **111**, 096803 (2013).
[19] J. Jung and A. H. MacDonald, Phys. Rev. B **79**, 235433 (2009).
[20] T. Makarova and F. Palacio, *Carbon Based Magnetism: An Overview of the Magnetism of Metal Free Carbon-based Compounds and Materials* (Elsevier, Amsterdam, 2006).
[21] M. Wimmer, İ. Adagideli, S. Berber, D. Tománek, and K. Richter, Phys. Rev. Lett. **100**, 177207 (2008).
[22] C. Cocchi, D. Prezzi, A. Calzolari, and E. Molinari, J. Chem. Phys. **133**, 124703 (2010).
[23] W. L. Wang, O. V. Yazyev, S. Meng, and E. Kaxiras, Phys. Rev. Lett. **102**, 157201 (2009).
[24] Z. Bullard, E. C. Girão, J. R. Owens, W. A. Shelton, and V. Meunier, Sci. Rep. **5**, 7634 (2015).
[25] Z. H. Qiao, J. Jung, Q. Niu, and A. H. MacDonald, Nano Lett. **11**, 3453 (2011).
[26] Z. H. Qiao, J. Jung, C. W. Lin, Y. F. Ren, A. H. MacDonald, and Q. Niu, Phys. Rev. Lett. **112**, 206601 (2014).
[27] J. Hachmann, J. J. Dorando, M. Avilés, and G. K.-L. Chan, J. Chem. Phys. **127**, 134309 (2007).
[28] F. Plasser, H. Pašalić, M. H. Gerzabek, F. Libisch, R. Reiter, J. Burgdörfer, T. Müller, R. Shepard, and H. Lischka, Angew. Chem., Int. Ed. **52**, 2581 (2013).
[29] M. Golor, S. Wessel, and M. J. Schmidt, Phys. Rev. Lett. **112**, 046601 (2014).
[30] E. H. Lieb, Phys. Rev. Lett. **62**, 1201 (1989).
[31] J. A. Chan, B. Montanari, J. D. Gale, S. M. Bennington, J. W. Taylor, and N. M. Harrison, Phys. Rev. B **70**, 041403(R) (2004).
[32] L. Brey, H. A. Fertig, and S. Das Sarma, Phys. Rev. Lett. **99**, 116802 (2007).
[33] See Supplemental Material at http://link.aps.org/supplemental/10.1103/PhysRevLett.116.026802, which includes Refs. [34–40], for the details of theoretical and experimental methods as well as additional figures and discussions.
[34] P. E. Blöchl, Phys. Rev. B **50**, 17953 (1994).
[35] G. Kresse and J. Furthmüller, Phys. Rev. B **54**, 11169 (1996).
[36] G. Kresse and D. Joubert, Phys. Rev. B **59**, 1758 (1999).
[37] J. P. Perdew, K. Burke, and M. Ernzerhof, Phys. Rev. Lett. **77**, 3865 (1996).
[38] J. Tersoff and D. R. Hamann, Phys. Rev. Lett. **50**, 1998 (1983).
[39] J. Taylor, H. Guo, and J. Wang, Phys. Rev. B **63**, 245407 (2001).
[40] M. Brandbyge, J. L. Mozos, P. Ordejon, J. Taylor, and K. Stokbro, Phys. Rev. B **65**, 165401 (2002).
[41] C.-H. Park, L. Yang, Y.-W. Son, M. L. Cohen, and S. G. Louie, Nat. Phys. **4**, 213 (2008).
[42] B. Hunt, J. D. Sanchez-Yamagishi, A. F. Young, M. Yankowitz, B. J. LeRoy, K. Watanabe, T. Taniguchi, P. Moon, M. Koshino, P. Jarillo-Herrero, and R. C. Ashoori, Science **340**, 1427 (2013).
[43] J. Cai, P. Ruffieux, R. Jaafar, M. Bieri, T. Braun, S. Blankenburg, M. Muoth, A. P. Seitsonen, M. Saleh, X. Feng, K. Müllen, and R. Fasel, Nature (London) **466**, 470 (2010).
[44] Ph. Guaino, D. Carty, G. Hughes, O. McDonald, and A. A. Cafolla, Appl. Phys. Lett. **85**, 2777 (2004).
[45] D. F. Perepichka, M. Bendikov, H. Meng, and F. Wudl, J. Am. Chem. Soc. **125**, 10190 (2003).
[46] S. S. Zade, N. Zamoshchik, A. R. Reddy, G. Fridman-Marueli, D. Sheberla, and M. Bendikov, J. Am. Chem. Soc. **133**, 10803 (2011).
[47] P. Häberle, P. Fenter, and T. Gustafsson, Phys. Rev. B **39**, 5810 (1989).
[48] G. Z. Magda, X. Jin, I. Hagymási, P. Vanscó, Z. Osváth, P. Nemes-Incze, C. Hwang, L. P. Biró, and L. Tapasztó, Nature (London) **514**, 608 (2014).